energies

MDPI

Article

Novel Active Damping Design Based on a Biquad Filter for an LLCL Grid-Tied Inverter †

Bin Wang [1], Qiangsong Zhao [1,*], Gong Zhang [1], Hongwei Zhang [1], Kaiyue Liu [1] and Xuebin Yue [2]

[1] School of Electronic and Information, Zhongyuan University of Technology, Zhengzhou 450007, China
[2] Department of Electronic and Computer Engineering, Ritsumeikan University, Kusatsu 525-8577, Shiga, Japan
* Correspondence: zhaoqiangsong@126.com

† This paper is an extended version of our paper published in 2022 Asian Conference on Frontiers of Power and Energy (ACFPE), Chengdu, China, 21–23 October 2022; pp. 102–107.

Abstract: LLCL filters for grid-tied inverters have been adopted to get better performance for the harmonics near the switching frequency than commonly used LCL filters. However, the resonant peak caused by a pair of unstable resonance poles of the LLCL filters is introduced and makes the system become unstable. In this paper, a biquad filter composed of a notch filter and a resonator is introduced to restrain the resonant peak. In this method, the resonance point and the notch point of the biquad filter are placed at the appointed frequency, and the resonant peak is transferred to the stable area by phase transformation, so that the system does not cross −180° at the resonant peak. This method makes the system have higher control bandwidth and stronger robustness even in a weak power grid. Meanwhile, a proportional-integral multiresonant repetitive controller is used to restrain low-frequency current harmonics and improve the steady-state and dynamic performance of the control system. Furthermore, based on the active damping of the biquad filter, the stability criterion of the control system under a weak power grid is given. Finally, the accuracy of the analysis and the effectiveness of the method is verified by simulations.

Keywords: LLCL filter; grid-tied inverter; biquad filter; weak grids

Citation: Wang, B.; Zhao, Q.; Zhang, G.; Zhang, H.; Liu, K.; Yue, X. Novel Active Damping Design Based on a Biquad Filter for an LLCL Grid-Tied Inverter. *Energies* **2023**, *16*, 1093. https://doi.org/10.3390/en16031093

Academic Editors: Vítor Monteiro and Jelena Loncarski

Received: 22 November 2022
Revised: 30 December 2022
Accepted: 16 January 2023
Published: 19 January 2023

1. Introduction

Under the target of "double carbon", distributed generation system based on renewable energy such as wind, hydropower, and solar energy is an efficient way to relieve energy shortage and resolve environmental pollution problems [1–3]. Under above background, the grid-tied inverters (GTI) have been widely used [4]. It is widely believed that L filters or LCL filters are normally applied to suppress the high-frequency switching harmonics generated by GTI.

With the same filtering effect, the LCL filters need smaller volume and lower cost than L filters [5,6]. In [7], the LLCL filter topology is proposed to decrease the whole inductance. The series resonant branch of the LLCL filter is composed by connecting a small inductor in series to the filter capacitor branch. The resonant frequency is designed at the switching frequency (SF), which can better filter the harmonics at the SF. In contrast with the LCL filter with the same filtering effect, the inductance value of the LLCL filter is smaller [8]. But the LLCL filter still has its inherent resonant peak, which causes the instability of the GTI system. The stability of LLCL filter considering the effect of time delay was discussed in [9]. The results show that the sampling frequency of 1/6 ($f_s/6$) can be used as the critical resonant frequency of the LLCL filter. If this frequency is higher than ($f_s/6$), the damping method is not needed and the system is stable. Therefore, passive damping (PD) methods [10–12] and active damping (AD) methods [13–15] are usually used to restrain resonance, or hybrid damping methods combining PD methods and AD methods is applied [16].

Due to the efficiency problem, the AD method is considered a promising method to solve the resonance problem. Typical AD methods, such as capacitive-current feedback [13,14] or resonant-inductor-voltage feedback [15], compensate the control loop through feedback filter state variables. However, above schemes still need additional sensors, and they are easily affected by parameter changes and external interference. Reference [17,18] put forward to add notch filter (NF) to "leach resonance". By adapting the notch frequency, the resonant peak could be absolutely eliminated without any sensors. However, because of the aging of devices, the saturation of the magnetic core, the impedance variation of the grid, and other factors, the resonant frequency will change accordingly. An AD method of LLCL filter based on proportional resonance control is proposed in [19,20]. Similarly, this method also does not consider the change in grid impedance. In [21], the notch frequency of NF is designed to be higher than the resonant frequency of the LCL filter, and the phase of the LCL filter is pushed down by using the phase lag of NF, to avoid the crossing of $-180°$ at the resonant frequency and ensures the stability of the control system. However, the solution sacrifices part of the phase angle margin, and lowers the control bandwidth, so the performance of the control system will be dropped [22]. Because of the similarity between LLCL filters and LCL filters, the same problem will occur when this method is applied to the LLCL filter. Some researchers have advanced an adaptive filter to restrain resonance, but it ineluctably advances the quantity of calculation of the digital controller and limits the rise of the SF [23].

In consideration of the above theory, some literates have introduced a biquad filter (BF) [24], which is mainly to place the resonance point and notch point of BF at the appointed frequency and transfer the resonant peak to the stable region through a phase transition. In this way, the system will not pass through $-180°$ at the resonant peak. Because the BF enables the system to have higher control bandwidth and strong robustness even in the weak power grid environment, it is only briefly introduced in [25]. Therefore, the BF is used in this paper to suppress the resonant peak of the system. Meanwhile, proportional-integral multiresonant (PIMR) repetitive controller [26,27] is used as the current regulator without any sensors and resistors. Simulations show that the proposed algorithm is robust even in weak power grids.

This paper mainly includes the following contents: the second section mainly analyzes the topology of LLCL GTI and the comparative analysis of the filtering performance of LLCL filters and LCL filters. The third section introduces the BF and analyzes the working mechanism of BF to restrain resonance in the weak power grid. In the fourth section, the stability of the PIMR repetitive controller is analyzed, the method of selecting parameters is given, and the criterion of system stability under the weak power grid environment is improved. Finally, verified by simulation, it is proved that the proposed scheme is accurate and effective.

2. Mathematical Model of LLCL-Type Inverter

The LLCL GTI and its topology are shown in Figure 1. Where the inductor L_f and capacitor C_f form a series resonant branch; L_g is the equivalent grid impedance; the inductor on the inverter side and the inductor on the grid side are L_1 and L_2 respectively. The control system uses a phase-locked loop to obtain the grid-tied current instruction i_2^* synchronized with the grid voltage V_g. In the control algorithm module, PIMR repetitive controller $G_i(s)$ is used, the transfer function of it is

$$G_i(s) = G_{PIMR}(s) = K_p + \frac{K_i}{s} + \sum_{n=1}^{\infty} \frac{2K_r s}{s^2 + (n\omega_0)^2} \tag{1}$$

where K_r is gain of n-order resonance controller, $K_p = k_p - \frac{k_r}{2}$; $K_i = \frac{k_i}{T_0}$; k_p is the proportional controller gain, k_r is the repetitive controller gain, T_0 is fundamental period of the reference signal. G_n is the BF used to suppress the resonant peak of the LLCL filter. The control block diagram of the inverter system is shown in Figure 2. Because when digital

control is adopted in LLCL GTI, PWM modulation will introduce computation delay and modulation delay, which is represented by $G_d(s)$, and it can be approximated as

$$G_d(s) = e^{-1.5sT_s} \tag{2}$$

where T_s is the sampling period, $T_s = 1/f_s$, f_s is sampling frequency, f_s = 10 kHz. According to Figure 1, it could be inferred that the transfer function of the LLCL filter is

$$G_{LLCL}(s) = \frac{i_2}{u_{inv}} = \frac{L_f C_f s^2 + 1}{L_1 L_2 C_f s^3 + (L_1 + L_2) L_f C_f s^3 + (L_1 + L_2) s} \tag{3}$$

The resonant frequency of the LLCL filter is

$$f_{r\_LLCL} = \frac{1}{2\pi} \sqrt{\frac{L_1 + L_2}{(L_1 L_2 + L_1 L_f + L_2 L_f) C_f}} \tag{4}$$

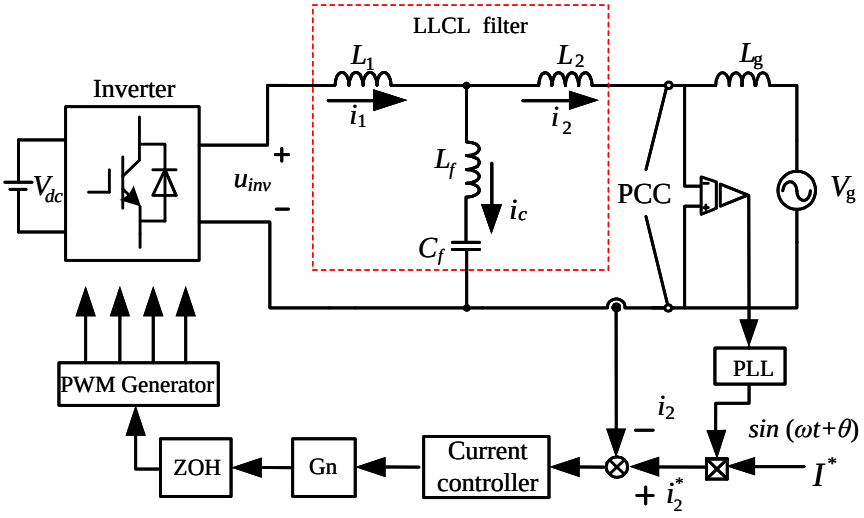

Figure 1. LLCL single-phase GTI and its topology.

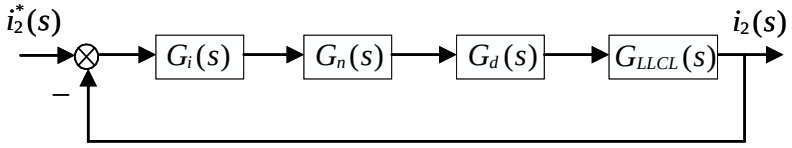

Figure 2. Control block diagram of the inverter system.

According to (3), the anti-resonant frequency of the LLCL filter is

$$f_{s\_LLCL} = \frac{1}{2\pi \sqrt{L_f C_f}} \tag{5}$$

Generally, the anti-resonant frequency is designed as the SF to suppress the switching harmonics [7].

When $L_f = 0$, the transfer function of the LCL filter can be obtained.

$$G_{LCL}(s) = \frac{1}{L_1 L_2 C_f s^3 + (L_1 + L_2) s} \tag{6}$$

The resonant frequency is

$$f_{r\_LCL} = \frac{1}{2\pi}\sqrt{\frac{L_1 + L_2}{L_1 L_2 C_f}} \tag{7}$$

From the transfer functions of the LCL filter and LLCL filter, their Bode diagrams are plotted in Figure 3. Since the value of L_f is extraordinarily little, the resonant frequencies of the LLCL filter and LCL filter are nearly equal. They have the same harmonic attenuation capacity of -20 dB/dec in the low-frequency band. In the middle-frequency band, they are both -60 dB/dec. The LCL filter still attenuates by -60 dB/dec in the high-frequency band, while the LLCL filter drops to -20 dB/dec. However, because of the existence of the LC resonant branch, the LLCL filter generates an anti-resonant peak at the SF, which advances the harmonic suppression performance of the filter. Therefore, the harmonic suppression capability of the LLCL filter is greater than that of the LCL filter.

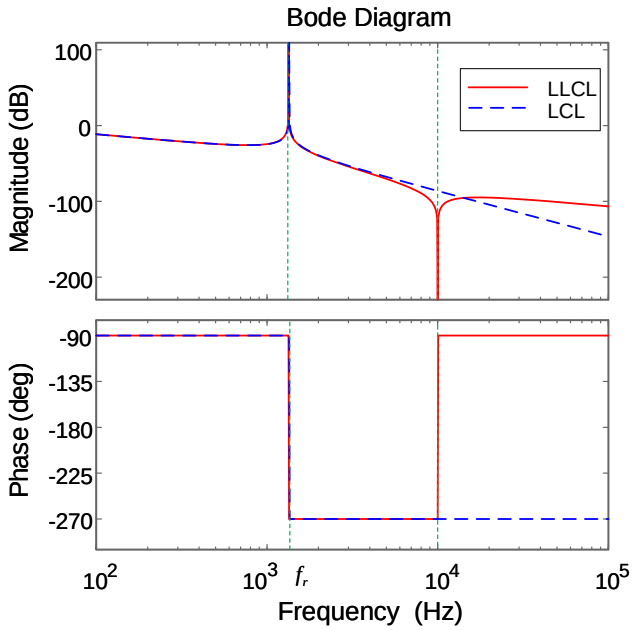

Figure 3. Bode diagrams of LCL filter and LLCL filter.

3. Suppression of Resonant Peak

A BF is used to suppress the resonant peak of the LLCL filter in the paper, and the expression in its complex domain is

$$G_{\mathrm{n}}(s) = \frac{\omega_p^2}{\omega_z^2}\frac{s^2 + \omega_z^2}{s^2 + \omega_p^2} \tag{8}$$

where $\omega_p = 2\pi f_p$ and $\omega_z = 2\pi f_z$ are a resonant pole and a notch point respectively, and a constant coefficient of ω_p^2/ω_z^2 is used to ensure the unit DC gain ($f_z < f_p$, $f_p > f_{\mathrm{s}}/6$). Usually, we use Tustin transformation to discretize NF and apply it to (8).

$$G_n(z) = G_n(s)|_{s=k\frac{z-1}{z+1}} = \frac{\omega_p^2}{\omega_z^2}\frac{(k^2+\omega_z^2) - 2(k^2-\omega_z^2)z^{-1} + (k^2+\omega_z^2)z^{-2}}{(k^2+\omega_p^2) - 2(k^2-\omega_p^2)z^{-1} + (k^2+\omega_p^2)z^{-2}} \tag{9}$$

where $k = \frac{2}{T_s}$, simplified (9) can be written as

$$G_n(z) = \frac{a_0 - a_1 z^{-1} + a_0 z^{-2}}{1 - b_1 z^{-1} + z^{-2}} \tag{10}$$

where a_0, a_1 and b_1 are the parameters of the BF, and they can be expressed as

$$a_0 = \frac{\omega_p^2}{\omega_z^2}\frac{k^2+\omega_z^2}{k^2+\omega_p^2}, \quad a_1 = \frac{\omega_p^2}{\omega_z^2}\frac{2(k^2-\omega_z^2)}{k^2+\omega_p^2}, \quad b_1 = \frac{2(k^2-\omega_p^2)}{k^2+\omega_p^2} \tag{11}$$

It should be pointed that, as shown in (11), the transfer function of the BF given by (10) is characterized by three parameters a_0, a_1, and b_1. Therefore, the BF could be easily implemented in a digital signal processor by using the Transposed Canonical Form, as it is shown in Figure 4.

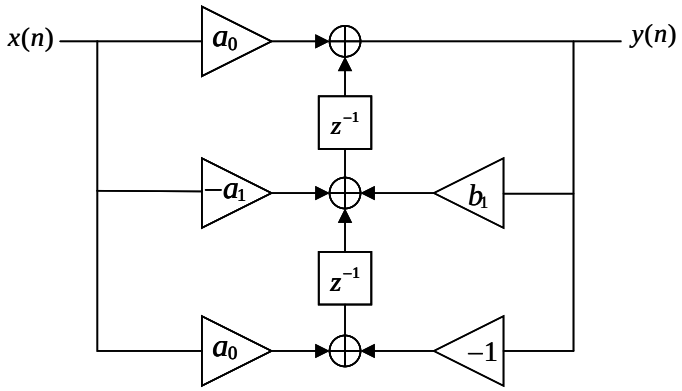

Figure 4. Transposed Canonical Form for the implementation of a digital BF.

The Bode diagram of the BF is plotted in Figure 5. It could be known that the BF generates grooves at f_z and resonance at f_p. Besides providing a phase lead of 180° in the frequency range of $f_z < f < f_p$, the BF also provides a phase of 0° in the range of $f < f_z$ and $f > f_p$. Since f_p is the target resonance frequency, it should be placed in the stable region, that is, $f_s/6 < f_p < f_s/2$. In order to suppress the resonant peak of the LLCL filter, it is only necessary to align the antiresonant peak f_z of the BF with the resonant peak f_r of the LLCL filter. But in fact, due to the uncertainty of power grid impedance, the f_r will change greatly, so it is hard to achieve $f_z = f_r$. Under this circumstances, the value of f_z can be appropriately reduced and need not be used to counteract the original resonant f_r, that is, $f_z < f_r$ could be satisfied, so that the BF invariably provides a 180° phase lead for the LLCL filter under the resonant frequency.

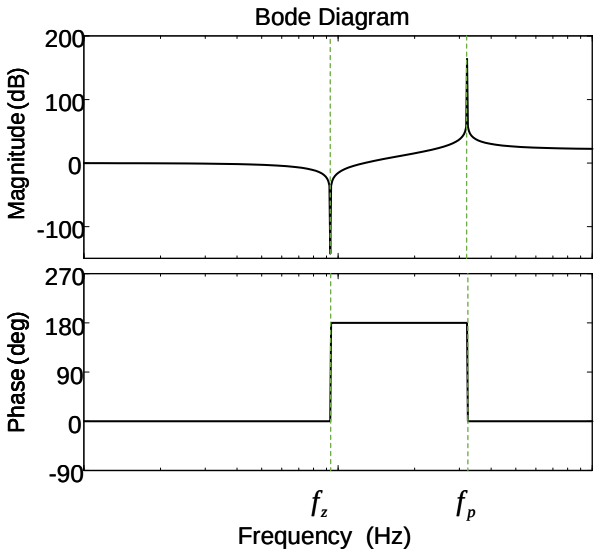

Figure 5. Bode diagram of the BF.

Due to the limited control bandwidth of the PIMR repetitive controller, the controller only has a great impact on the bandwidth and does not contribute significantly to the frequency outside the bandwidth. Therefore, the PIMR repetitive controller can be regarded as a proportional gain to evaluate the stability in the high-frequency band, which could be assumed $G_i(s) \approx c$ and c is a constant. According to (12), the loop gain of the filter with and without BF could be plotted, as shown in Figures 6 and 7. Figure 6 plots the Bode diagram of loop gain and the BF when the notch point of the BF is aligned with the resonant peak of the filter without considering the change of grid impedance, and Figure 7 shows the Bode diagram of loop gain and the BF when the notch point of the BF is not aligned with the resonant peak of the LLCL filter. Table 1 gives the parameters of a single-phase LLCL GTI.

$$T_{i2}(s) = G_i(s)G_n(s)G_d(s)G_{LLCL}(s) \tag{12}$$

$$\begin{aligned} \omega_{z-\min} &= \lim_{L_g \to \infty} \sqrt{\frac{L_1 + L_2 + L_g}{(L_1(L_2 + L_g) + L_1 L_f + (L_2 + L_g)L_f)C_f}} \\ &= \frac{1}{\sqrt{(L_1 + L_f)C_f}} \end{aligned} \tag{13}$$

Table 1. Control parameters of the main circuit.

Parameters	Value
input voltage V_{dc}/V	380
grid voltage U_g/V	220
frequency f_0/Hz	50
switching frequency f_{sw}/kHz	10
inverter side inductance L_1/mH	3.8
grid side inductance L_2 /mH	2.2
capacitor C_f/μF	10
filter inductance L_f/μH	25.33
sampling frequency f_s/ kHz	10

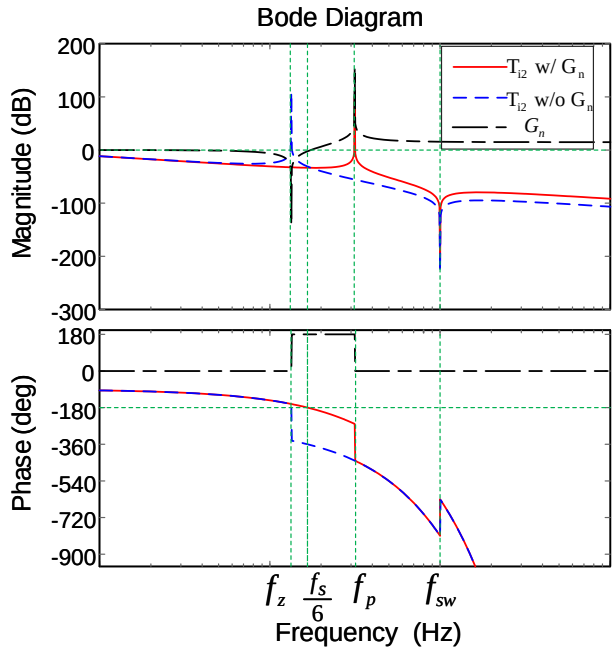

Figure 6. Bode diagram of loop gain and the BF at $f_z = f_r$.

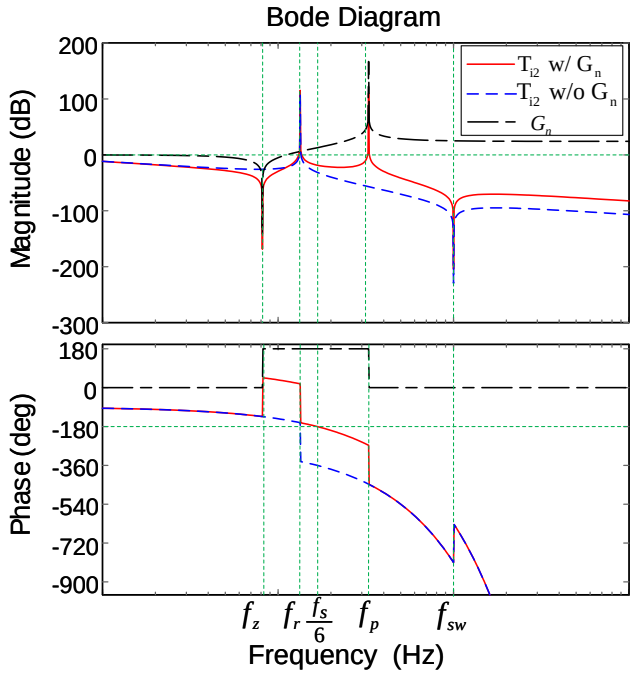

Figure 7. Bode diagram of loop gain and the BF at $f_z < f_r$.

As shown in Figure 6, when BF is not added, $G_n(s)$ can be seen as constant. $T_{i2}(s)$ traverses $-180°$ at f_r and has an infinite resonant peak. When the BF is added, because the BF provides a 180° phase lead, the phase diagram of $T_{i2}(s)$ no longer traverses $-180°$ at f_r, and the $-180°$ crossover is increased from the original f_r to $f_s/6$. When grid impedance is considered, the resonant frequency of the system becomes smaller, as shown in Figure 7. f_z is usually set to the minimum value that f_r could achieve to ensure the system is robust enough. It is known from (13) that when L_g is infinity, f_z is the minimum.

Figure 8 is the system Bode diagram when $L_g = 2$ mH, 4 mH, and 6 mH. It can be known from the figure that their amplitude margins are 26.7 dB, 24.3 dB, and 22.9 dB at $f_s/6$ respectively when $L_g = 2$ mH, 4 mH, and 6 mH. And all three of them have a phase margin of 23°, so the control system can remain stable.

According to the above analysis, we could know that the BF must satisfy the stability at $f_p > f_s/6$ and $f_z \leq f_r$.

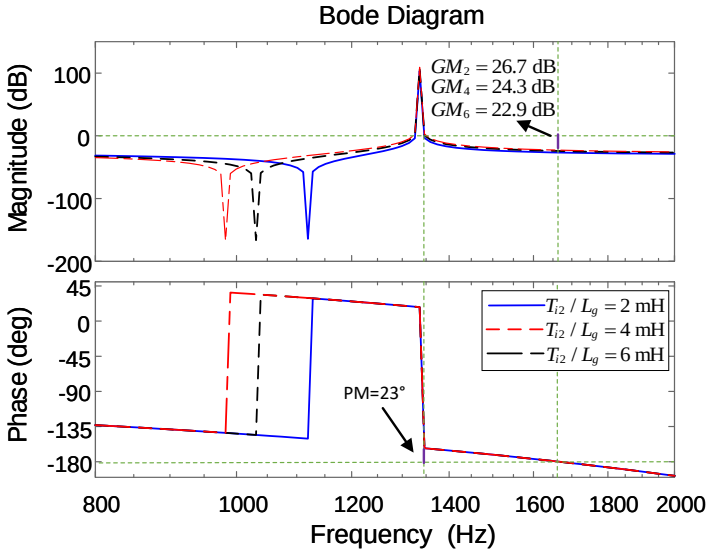

Figure 8. System Bode diagram when $L_g = 2$ mH, 4 mH and 6 mH.

4. Stability Analysis of Current Controller under the BF

The grid current contains a lot of low-frequency harmonics in the GTI system, so it is essential to choose the appropriate current controller to dispose of it. Because the PIMR repetitive controller has strong harmonic suppression capacity and great dynamic performance, the PIMR repetitive controller is selected in this paper. The controller consists of a repetitive controller in parallel with a proportional gain controller, which reduces a large number of parameters of the traditional proportional multi-resonant controller, its expression in the discrete domain is

$$G_{PIMR} = k_p + G_{Qrc} = k_p + \frac{Q(z)z^{-N}}{1 - Q(z)z^{-N}} z^{-m} k_r S(z) \tag{14}$$

As shown in Figure 9, $Q(z)$ is an internal function and is constant in the paper, that is $Q(z) = 0.97$. The main purpose of the existence of $Q(z)$ is to increase the peak gain of the repetitive controller at a high-frequency range, to improve the stability of the system. $N = f_s/f_0$, N refers to the sampling times in each period, f_0 refers to the fundamental frequency of power grid. z^m is the phase advance compensator. $S(z)$ is a low-pass filter for attenuating high-frequency signals. As shown in (15), $P(z)$ is the controlled object, which refers to the product of the LLCL filter and BF in the paper, that is

$$P(z) = G_n(z) G_{LLCL}(z) \tag{15}$$

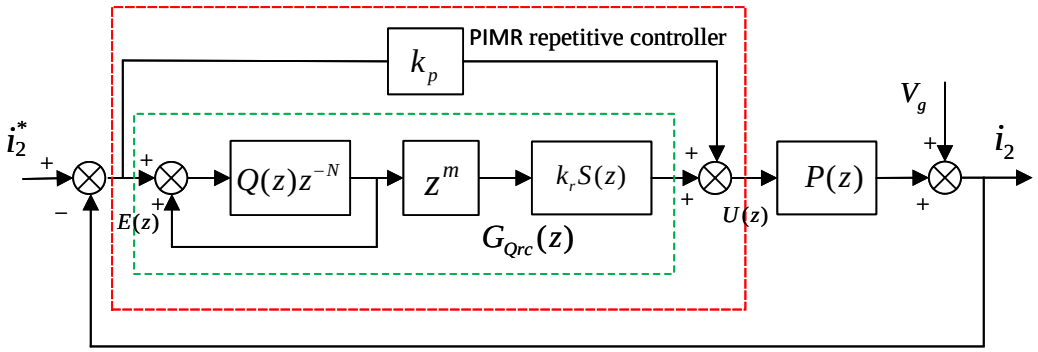

Figure 9. System diagram of PIMR repetitive controller.

The discrete repetitive control expression is

$$G_{Qrc}(z) = \frac{Q(z)z^{-N}}{1 - Q(z)z^{-N}} z^{-m} k_r S(z) \tag{16}$$

The tracking error of the system is

$$E(z) = \frac{1}{1 + [G_{Qrc}(z) + k_p]P(z)} [i_2^* - V_g(z)] \tag{17}$$

The characteristic polynomial is

$$\begin{aligned} 1 + [G_{Qrc}(z) + k_p]P(z) &= 1 + G_{Qrc}(z)P(z) + k_p P(z) \\ &= [1 + k_p P(z)][1 + \frac{G_{Qrc}(z)P(z)}{1 + k_p P(z)}] \\ &= [1 + k_p P(z)][1 + G_{Qrc}(z)P_0(z)] \end{aligned} \tag{18}$$

$$P_0(z) = \frac{P(z)}{1 + k_p P(z)} \tag{19}$$

The system will be in a stable state if the following two conditions are met.

①: All roots of $1+k_pP(z)=0$ are in the unit circle.
②: $[1+G_{Qrc}(z)P_0(z)] \neq 0$.
Substitute (16) into ②, We can get the following:

$$\left|1-Q(z)z^{-N}+Q(z)z^{-N+m}k_rS(z)P_0(z)\right| \neq 0 \tag{20}$$

To be satisfied (20), it needs to be satisfied

$$\left|Q(z)z^{-N}[1-z^mk_rS(z)P_0(z)]\right| < 1(\forall z=e^{st}=e^{j\omega t}, 0<\omega<\pi/T) \tag{21}$$

Because the frequency of the reference signal and the interference signal is an integral multiple of the fundamental frequency, (22) could be get by substituting $\left|z^{-N}\right|=1$ into (21)

$$|Q(z)[1-k_rz^mS(z)P_0(z)]|<1 \tag{22}$$

According to the frequency characteristic:

$$P_0(j\omega)=N_p(\omega)\exp(j\theta_p(w)) \tag{23}$$

where $N_p(\omega)$ and $\theta_p(\omega)$ are the amplitude-frequency characteristics and phase-frequency characteristics of the $P(z)$ respectively.
Substitute $P_0(z)$ and $S(z)$ into (22), We can get the following:

$$\left|1-k_rN_p(\omega)N_s(\omega)e^{j[\theta_s(\omega)+\theta_p(\omega)+m\omega]}\right|<1 \tag{24}$$

The exponential function e is expanded according to the Euler formula, (24) could be expressed as

$$k_rN_p(\omega)N_s(\omega)<2\cos[\theta_s(\omega)+\theta_p(\omega)+m\omega] \tag{25}$$

Due to $N_p(\omega)>0$, $N_s(\omega)>0$, (25) necessarily requires that is

$$\left|\theta_s(\omega)+\theta_p(\omega)+m\omega\right|<90^\circ \tag{26}$$

$$0<k_r<\min\frac{2\cos[\theta_s(\omega)+\theta_p(\omega)+m\omega]}{N_p(\omega)N_s(\omega)} \tag{27}$$

The system is stable when k_r and m satisfy (26) and (27). Formula (26) contains only one parameter m, so the value of m could be confirmed first, and then the value of k_r could be confirmed by (27). The value of k_p could be confirmed by condition ①, and the fourth-order Butterworth filter $S(z)$ is selected in the paper. The cutoff frequency of it is 1 kHz, that is

$$S(z)=\frac{0.004824z^4+0.0193z^3+0.02895z^2+0.0193z+0.004824}{z^4-2.37z^3+2.314z^2-1.055z+0.1874} \tag{28}$$

According to [26], they could be acquired as follows: $k_p=5$, $k_r=3$, $m=7$.
With increasing grid-tied power, the power grid is getting weaker and weaker, which has a great impact on the performance of GTI. Therefore, the designed control system should have strong robustness in response to the changes in grid impedance. If the impedance of the power grid changes, it could be seen from the analysis in the second section that the resonance zero point f_z of the BF should be designed at the minimum value that can be attained by the resonance point f_r of the LLCL filter, so the system is stable. According to (22), we define

$$H(e^{j\omega})=|Q(z)[1-k_rz^mS(z)P_0(z)]|, z=e^{st}=e^{j\omega t} \tag{29}$$

If $H(e^{j\omega})<1$, the end of vector $H(e^{j\omega})$ is in the unit circle, which means the system is stable [26]. Because $H(e^{j\omega})<1$ is the stability criterion of the whole system, it is

necessary to regard the calculation delay of z^{-1}, so that $P_1(z) = P_0(z)z^{-1}$, the stability criterion becomes

$$H_1(e^{j\omega}) = |Q(z)[1 - k_r z^m S(z)P_1(z)]| \tag{30}$$

Therefore, $H(e^{j\omega}) < 1$ could be used as the stability criterion of the whole system. When $L_g = 2$ mH, 4 mH, and 6 mH, the trajectory of $H_1(e^{j\omega})$ is plotted in Figure 10, it is easy to see that the trajectories are all in the unit circle. Therefore, the proposed control scheme is robust to the variety of power grid impedance.

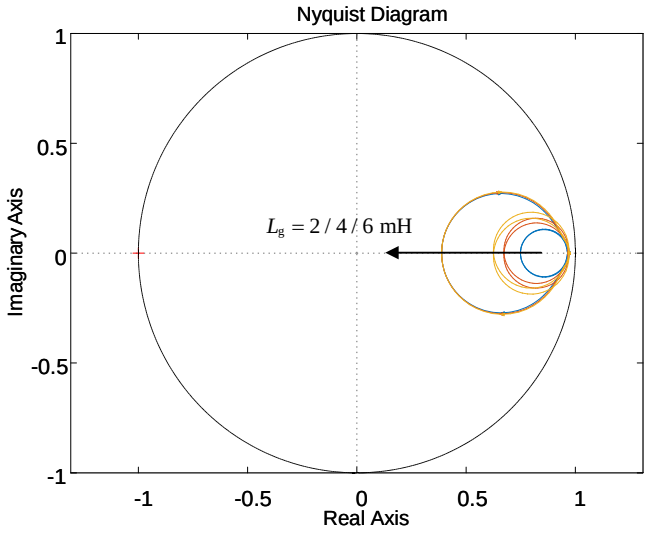

Figure 10. The trajectory of $H_1(e^{j\omega})$ with $L_g = 2$ mH, 4 mH and 6 mH.

5. Simulation Verification

To testify to the feasibility of the theoretical analysis, the model of the LLCL inverter shown in Figure 1 is built by MATLAB/Simulink and the simulation analysis is conducted. The simulation parameters are shown in Table 1.

Figure 11 is the grid-tied current waveform before and after the control switch. From Figure 11, at the beginning, it is cut to the state of the BF, the grid-tied current waveform is smooth, and the system remains stable. When the system is cut to the state without BF, the grid-tied current begins to oscillate and the system rapidly loses stability. Therefore, the proposed BF can suppress the resonance and make the system stable.

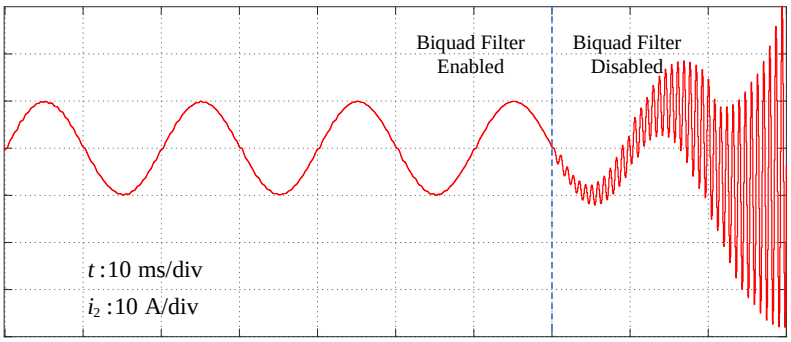

Figure 11. Grid-tied current waveform before and after control switch.

Figures 12 and 13 are the Fourier analysis of the grid-tied current of the LLCL filter and LCL filter under BF respectively. By comparing the Total Harmonic Distortion (THD) of the two figures, we could see that the filtering effect of LLCL GTI is better. And the high-frequency harmonic content of the grid-tied current of the LCL filter at the SF is 0.06%, while that of the LLCL filter is less than 0.001%. It could be known that the high-frequency

harmonics at the SF are effectively filtered out by series branches of the LLCL filter, and the low-frequency harmonics are suppressed by PIMR repetitive controller. Figure 14 plots grid voltage and current waveforms of LLCL filter with $L_g = 0$ mH. From Figure 14, the grid-connected current waveform has no large fluctuation and distortion, and the grid voltage and the grid current is in the same phase. Therefore, the proposed control strategy can make the system have better steady-state performance.

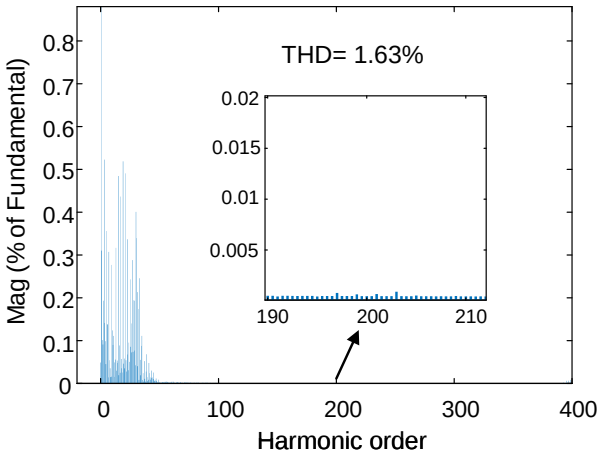

Figure 12. FFT analysis of LLCL grid-tied current with $L_g = 0$ mH.

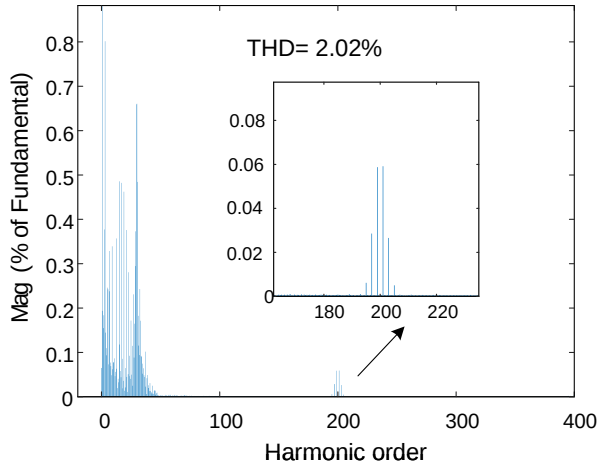

Figure 13. FFT analysis of LCL grid-tied current with $L_g = 0$ mH.

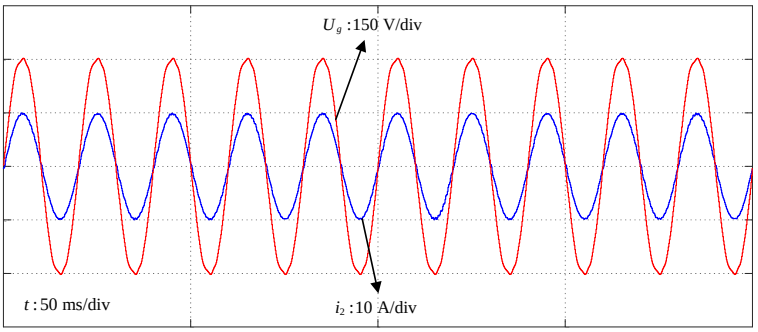

Figure 14. Grid voltage and current waveforms of LLCL filter with $L_g = 0$ mH.

Figures 15–17 show the Grid-tied current waveform before and after the control switch with L_g = 2 mH, 4 mH and 6 mH. The THD of the three cases is 1.52%, 1.47%, and 1.49%, respectively. From the THD value, it can be seen that the value of THD is lower than the international standard, so the BF method can reduce the adverse impact of power grid impedance to a certain extent. At the same time, it could be known that when the BF is enabled, the waveform of the grid current is smooth, and when the BF is disabled, the current waveform rapidly oscillates and becomes unstable. This verifies that the proposed control strategy is still valid even in the weak power grids.

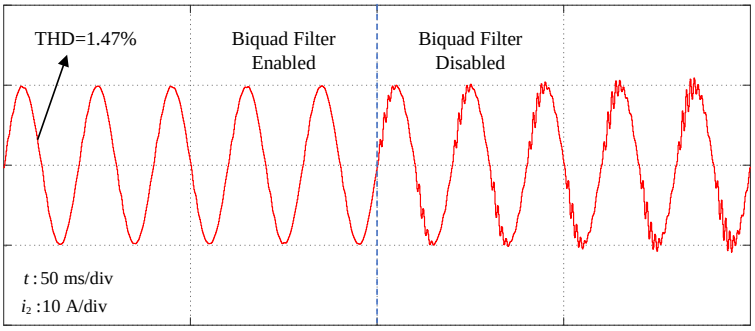

Figure 15. Grid-tied current waveform before and after control switch with L_g = 2 mH.

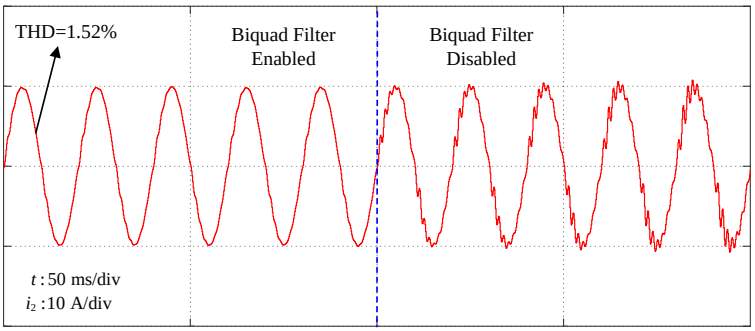

Figure 16. Grid-tied current waveform before and after control switch with L_g = 4 mH.

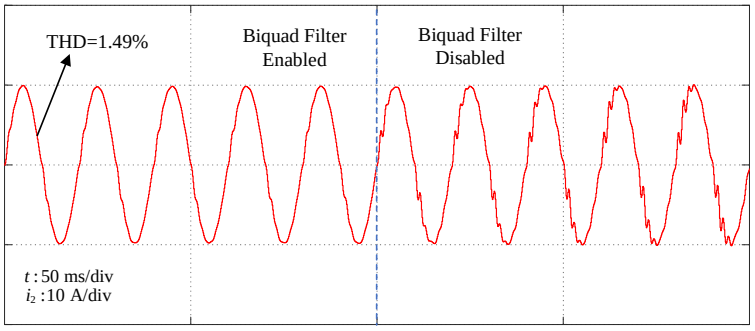

Figure 17. Grid-tied current waveform before and after control switch with L_g = 6 mH.

According to different grid impedances, the impedance values are switched every 50 ms to obtain the grid voltage and current waveforms as shown in Figure 18. By switching between different L_g, it could be known that grid voltage and current waveforms are smooth and basically unchanged even at the moment of switching, it could be confirmed that even in the weak power grids, the system can also show excellent performance and have strong robustness.

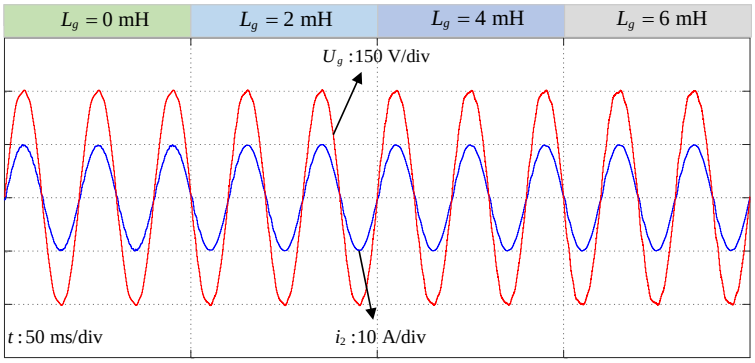

Figure 18. Simulation waveform of control system when power grid impedance changes.

Figure 19 shows the simulation results of power grid current under a given sudden change of current value. It is shown that when the given current suddenly changes from 5 A to 10 A, the grid-tied current can quickly track the given value and complete the mutation in only 60 ms, which is in line with our expectations, so it can be determined that the proposed control strategy has a rapid convergence speed and great dynamic performance.

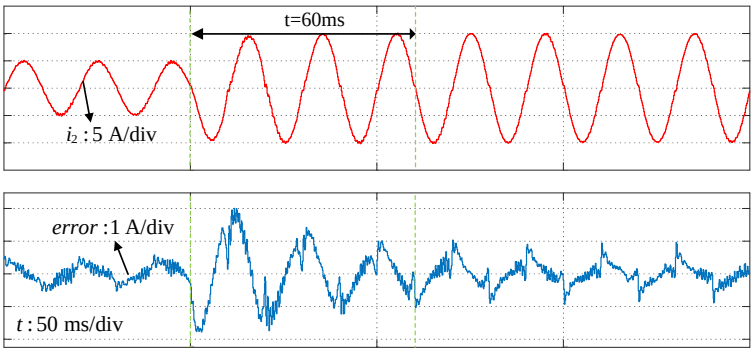

Figure 19. Grid current waveform under given current value.

6. Conclusions

In the paper, an AD method is advanced to restrain the resonant peak by BF composed of resonance and filtering. This method could efficiently transfer the resonant peak to the stable region, so that the system does not cross −180° at the resonant frequency. Meanwhile, PIMR repetitive controller is adopted in this paper, and the controller parameters are selected after strict theoretical demonstration. Through theoretical and simulation analysis, it is proved that the system still has strong robustness even in weak power grids.

Author Contributions: Conceptualization, B.W. and Q.Z.; methodology, B.W. and G.Z.; software, G.Z. and H.Z.; validation, X.Y. and G.Z.; formal analysis, Q.Z. and B.W.; investigation, K.L.; resources, Q.Z. and X.Y.; writing—original draft preparation, B.W.; writing—review and editing, B.W., Q.Z., G.Z., K.L., X.Y. and H.Z.; visualization, K.L. and H.Z.; supervision, Q.Z.; project administration, Q.Z. and X.Y. All authors have read and agreed to the published version of the manuscript.

Funding: This work was supported in part by the National Natural Science Foundation of China under Grant 61973157, in part by the Key Technologies Research and Development Program of Henan under Grant 222102210016, and in part by the Incubation Program for Young Master Supervisor under Grant D202213.

Data Availability Statement: The study did not report any data.

Conflicts of Interest: The authors declare no conflict of interest.

Abbreviations

The following abbreviations are used in this manuscript:

GTI	Grid-Tied Inverter
PD	Passive Damping
AD	Active Damping
NF	Notch Filter
SF	Switching Frequency
BF	Biquad Filter
PIMR	Proportional-Integral Multiresonant
THD	Total Harmonic Distortion

References

1. Han, J.; Hong, Q.; Feng, Z.; Syed, M.H.; Burt, G.M.; Booth, C.D. Design and implementation of a real-time hardware-in-the-loop platform for prototyping and testing digital twins of distributed energy resources. *Energies* **2022**, *15*, 6629. [CrossRef]
2. López-Prado, J.L.; Vélez, J.I.; Garcia-Llinás, G.A. Reliability Evaluation in Distribution Networks with Microgrids: Review and Classification of the Literature. *Energies* **2020**, *13*, 6189. [CrossRef]
3. Gallagher, K.S.; Zhang, F.; Orvis, R.; Rissman, J.; Liu, Q. Assessing the Policy gaps for achieving China's climate targets in the Paris Agreement. *Nat. Commun.* **2019**, *10*, 1256. [CrossRef] [PubMed]
4. Ilyushin, P.; Volnyi, V.; Suslov, K.; Filippov, S. Review of Methods for Addressing Challenging Issues in the Operation of Protection Devices in Microgrids with Voltages of up to 1 kV That Integrates Distributed Energy Resources. *Energies* **2022**, *15*, 9186. [CrossRef]
5. Xie, C.; Zhao, X.; Li, K.; Zou, J.; Guerrero, J.M. A new tuning method of multiresonant current controllers for grid-connected voltage source converters. *IEEE J. Emerg. Sel. Top. Power Electron.* **2019**, *7*, 458–466. [CrossRef]
6. Bolsi, P.C.; Prado, E.O.; Sartori, H.C.; Lenz, J.M.; Pinheiro, J.R. LCL Filter Parameter and Hardware Design Methodology for Minimum Volume Considering Capacitor Lifetimes. *Energies* **2022**, *15*, 4420. [CrossRef]
7. Wu, W.; He, Y.; Blaabjerg, F. An LLCL power filter for single-phase grid-tied inverter. *IEEE Trans. Power Electron.* **2012**, *27*, 782–789. [CrossRef]
8. Wu, W.; Huang, M.; Blaabjerg, F. Efficiency comparison between the LLCL and LCL-filters based single-phase grid-tied inverters. *Arch. Electr. Eng.* **2014**, *63*, 63–79. [CrossRef]
9. Huang, M.; Wang, X.; Loh, P.C.; Blaabjerg, F.; Wu, W. Stability analysis and active damping for llcl-filter-based grid-connected inverters. *IEEJ J. Ind. Appl.* **2015**, *4*, 187–195. [CrossRef]
10. Wu, W.; He, Y.; Tang, T.; Blaabjerg, F. A new design method for the passive damped LCL and LLCL filter-based single-phase grid-tied inverter. *IEEE Trans. Ind. Electron.* **2013**, *60*, 4339–4350. [CrossRef]
11. Wu, W.; Sun, Y.; Huang, M.; Wang, X.; Wang, H.; Blaabjerg, F.; Liserre, M.; Chung, H.S.h. A robust passive damping method for LLCL-filter-based grid-tied inverters to minimize the effect of grid harmonic voltages. *IEEE Trans. Power Electron.* **2013**, *29*, 3279–3289. [CrossRef]
12. Wu, W.; Huang, M.; Sun, Y.; Wang, X.; Blaabjerg, F. A composite passive damping method of the LLCL-filter based grid-tied inverter. In Proceedings of the 2012 3rd IEEE International Symposium on Power Electronics for Distributed Generation Systems (PEDG), Aalborg, Denmark, 25–28 June 2012; pp. 759–766.
13. Wu, L.; Liu, T.; Hao, X. Coordination control strategy for LLCL-filter based grid-tied inverter with indirect sliding mode power control and virtual impedance. *J. Eng.* **2019**, *2019*, 2804–2809. [CrossRef]
14. Khan, A.; Gastli, A.; Ben-Brahim, L. Modeling and control for new LLCL filter based grid-tied PV inverters with active power decoupling and active resonance damping capabilities. *Electr. Power Syst. Res.* **2018**, *155*, 307–319. [CrossRef]
15. Huang, M.; Wang, X.; Loh, P.C.; Blaabjerg, F. Resonant-inductor-voltage-feedback active damping based control for grid-connected inverters with LLCL-filters. In Proceedings of the 2014 IEEE Energy Conversion Congress and Exposition (ECCE), Pittsburgh, PA, USA, 14–18 September 2014; pp. 1194–1201.
16. Wu, W.; Lin, Z.; Sun, Y.; Wang, X.; Huang, M.; Wang, H.; Chung, H.S.H. A hybrid damping method for LLCL-filter based grid-tied inverter with a digital filter and an RC parallel passive damper. In Proceedings of the 2013 IEEE Energy Conversion Congress and Exposition, Denver, CO, USA, 15–19 September 2013; pp. 456–463.
17. Gonçalves, D.; Farias, J.V.M.; Pereira, H.A.; Luiz, A.S.A.; Stopa, M.M.; Cupertino, A.F. Design of Damping Strategies for LC Filter Applied in Medium Voltage Variable Speed Drive. *Energies* **2022**, *15*, 5644. [CrossRef]
18. Zhang, S.; Jiang, S.; Lu, X.; Ge, B.; Peng, F.Z. Resonance issues and damping techniques for grid-connected inverters with long transmission cable. *IEEE Trans. Power Electron.* **2014**, *29*, 110–120. [CrossRef]
19. Alemi, P.; Lee, D.C. Active damping control of LLCL filters based on virtual resistor for T-type three-level PWM converters. In Proceedings of the 2014 IEEE Energy Conversion Congress and Exposition (ECCE), Pittsburgh, PA, USA, 14–18 September 2014; pp. 2241–2248.
20. Alemi, P.; Bae, C.J.; Lee, D.C. Resonance suppression based on PR control for single-phase grid-connected inverters with LLCL filters. *IEEE J. Emerg. Sel. Top. Power Electron.* **2016**, *4*, 459–467. [CrossRef]

21. Yao, W.; Yang, Y.; Zhang, X.; Blaabjerg, F.; Loh, P.C. Design and analysis of robust active damping for LCL filters using digital notch filters. *IEEE Trans. Power Electron.* **2017**, *32*, 2360–2375. [CrossRef]
22. Yao, W.; Yang, Y.; Xu, Y.; Blaabjerg, F.; Liu, S.; Wilson, G. Phase reshaping via all-pass filters for robust LCL-filter active damping. *IEEE Trans. Power Electron.* **2020**, *35*, 3114–3126. [CrossRef]
23. Jing, Y.; Al Durra, A.; El-Saadany, E.F. An adaptive digital notch filter based on grid impedance estimation for improving LCL filter peformance. In Proceedings of the 2018 IEEE/PES Transmission and Distribution Conference and Exposition (T&D), Denver, CO, USA, 16–19 April 2018; pp. 1–5.
24. Akhavan, A.; Vasquez, J.C.; Guerrero, J.M. A robust method for controlling grid-connected inverters in weak grids. *IEEE Trans. Circuits Syst. II Express Briefs* **2020**, *68*, 1333–1337. [CrossRef]
25. Wang, B.; Ye, Y.; Zhao, Q.; Zhang, G. Active Damping Design of LLCL Grid-Connected Inverter Based on Biquad Filter. In Proceedings of the 2022 Asian Conference on Frontiers of Power and Energy (ACFPE), Chengdu, China, 21–23 October 2022; pp. 102–107.
26. Zhao, Q.; Ye, Y. A PIMR-Type Repetitive Control for a Grid-Tied Inverter: Structure, Analysis, and Design. *IEEE Trans. Power Electron.* **2018**, *33*, 2730–2739. [CrossRef]
27. Zhao, Q.; Zhang, H.; Gao, Y.; Chen, S.; Wang, Y. Novel Fractional-Order Repetitive Controller Based on Thiran IIR Filter for Grid-Connected Inverters. *IEEE Access* **2022**, *10*, 82015–82024. [CrossRef]